2021 IEEE Conference on Control Technology and Applications (CCTA).
August 8-11, 2021. San Diego, California

2021 IEEE Conference on Control Technology and Applications (CCTA).
August 8-11, 2021. San

Robust Nonlinear Control of the Minimum Safety Factor in Tokamaks

Andres Pajares and Eugenio Schuster

2021 IEEE Conference on Control Technology and Applications (CCTA) | 978-1-6654-3643-4/21/$31.00 ©2021 IEEE | DOI: 10.1109/CCTA48906.2021.9659126

***Abstract*— Tokamaks are torus-shaped devices whose goal is to produce energy by means of thermonuclear fusion reactions. This is achieved by using helical magnetic fields to confine a plasma, i.e., a very hot ionized gas, so that the necessary conditions for fusion (i.e., high pressure and confinement time) are achieved. The safety factor is a measure of the pitch of the magnetic-field lines, and plays an important role in the magnetohydrodynamic stability and confinement properties of the plasma. In particular, the minimum value of the safety factor across the plasma spatial domain is often closely related to the maximum achievable plasma pressure. In this work, a robust, nonlinear, model-based controller for the regulation of the minimum safety factor is presented. The controller is synthesized via Lyapunov theory, and robustified against model uncertainties by means of Lyapunov redesign techniques. The controller is tested, together with a controller for the plasma thermal energy, in one-dimensional simulations using COTSIM (Control Oriented Transport SIMulator) for a DIII-D scenario.**

I. Introduction

In a tokamak [1], a gas composed of hydrogen isotopes (normally deuterium, sometimes a mix of deuterium and tritium) is injected and heated up to temperatures on the order of tens of millions of degrees. This high temperature turns the gas into a plasma, i.e., its ions and electrons are dissociated. These charged particles, composing the plasma, are responsive to magnetic fields. Such property is the basis of the tokamak design, which employs helical magnetic fields to confine the plasma. When the appropriate confinement conditions are achieved, i.e., high enough pressure and confinement time, nuclear-fusion reactions happen within the plasma, releasing energy in the process. This nuclear-fusion energy can be employed to produce electricity while avoiding some of the inconveniences associated with fossil energy (like greenhouse-gas emissions), nuclear-fission energy (like long-lived radioactive waste), and renewable (solar or wind) energy (like relatively low power density and intermittency).

The safety factor, q, is a measure of the pitch of the magnetic-field lines within a tokamak. It varies in space from the magnetic axis (i.e., approximately the geometric axis of the tokamak torus) till the plasma edge (as depicted in Fig. 1 and 2). Therefore, q is in fact a space-dependent variable whose spatial shape is referred to as "profile." The q profile is closely related to the macroscopic stability of the plasma, also known as magnetohydrodynamic (MHD) stability [1], as well as to the microscopic behavior of the plasma, which determines the overall plasma-confinement levels in the absence of MHD instabilities. An example of MHD instability is the neoclassical tearing mode (NTM), which limits the achievable plasma pressure and, in some cases, can terminate the confined plasma. The NTMs are found at rational surfaces, i.e., surfaces defined by points with $q = m/n$, where the integers m and n are the poloidal and toroidal mode numbers, respectively. Increasing q removes low-order (i.e., low m) rational surfaces from the plasma and, therefore, avoids the development of the associated NTMs. On the other hand, a reduction of the microscopic plasma turbulence, with an associated confinement improvement, is found when internal transport barriers (ITBs) form in tokamaks. The ITB formation is sometimes triggered when the spatial derivative of q becomes low or negative in the central region of the plasma, i.e., near the magnetic axis (see Fig. 1). This implies that the minimum of the q profile across the plasma spatial domain is found somewhere between the magnetic axis and the plasma edge (see Fig. 2). As a result, active control of the minimum (in space) of the safety factor, q_{min}, may be highly beneficial to avoid MHD instabilities and maximize plasma confinement in tokamaks.

Extensive research has been carried out to develop algorithms for the regulation of the q profile (examples can be found in [2], [3], [4], [5]), sometimes in conjunction with β_N (see, for example, [6], [7], [8]). However, not much work can be found for the regulation of q_{min}. In [9], a proportional controller was designed for the regulation of q_{min}, and tested in the DIII-D tokamak. The controller makes use of the neutral beam injectors (NBIs) to regulate q_{min} by modifying the plasma resistivity, η. The control model does not account for q_{min} variations due to localized NBI current drive. Other pieces of work, like [10] or [11], consider regulation of the central safety factor, q_0, which corresponds to the value of q at the magnetic axis. In plasmas where the q profile is monotonically increasing from the magnetic axis till the plasma edge, it is found that $q_0 \equiv q_{min}$, so the algorithms proposed in [10], [11] would in fact regulate q_{min} (see Fig. 2). However, in general, these algorithms do not ensure q_{min} regulation because $q_0 \neq q_{min}$ is often found in tokamak-plasma scenarios of interest.

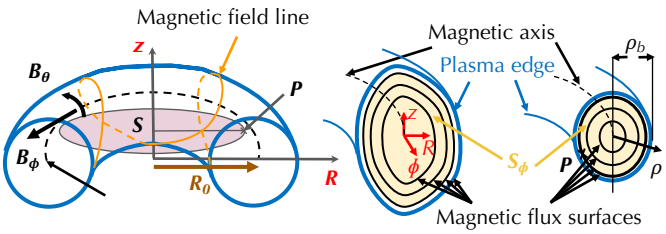

Fig. 1. Helical magnetic fields confine a plasma in tokamaks. This results in toroidally-nested magnetic-flux surfaces in the absence of MHD instabilities.

This work was supported in part by the U.S. Department of Energy (DE-SC0010661). A. Pajares (andres.pajares@lehigh.edu) and E. Schuster are with the Department of Mechanical Engineering and Mechanics, Lehigh University, Bethlehem, PA 18015, USA.

In this work, a novel controller for the regulation of q_{min} is presented. The lack of previous work on q_{min} regulation responds to the challenges associated with its time-varying location, i.e. the location of q_{min} in space, denoted by $\hat{\rho}_{q_{min}}$ in this work, varies in time as q_{min} is regulated. Lyapunov theory [12] has been employed to achieve a nonlinear-control design that retains as much information about the q-profile dynamics model as possible. In addition, Lyapunov-redesign techniques [12] have been utilized to robustify the design against model uncertainties. The particular design of this q_{min} controller allows for its integration with other controllers for the simultaneous regulation of different plasma properties [13]. A procedure to integrate the q_{min} controller with a controller for the thermal energy, W, is illustrated in this paper. The overall scheme has been tested for a DIII-D scenario in simulations using COTSIM (Control-Oriented Transport SIMulator), which employs plasma models that are one-dimensional (1D) in space. These simulation models are significantly more complex than those employed for control synthesis. This represents a significant test for the robustness of the controller against unknown dynamics. The actuators considered are the NBIs (which, in the DIII-D case, can drive localized current on the magnetic axis or off-axis) and electron-cyclotron heating and current drive (ECH&CD).

The paper is organized as follows. The control-synthesis model is described in Section II. The control synthesis is presented in Section III. A 1D-simulation study in a DIII-D scenario is included in Section IV. Finally, conclusions and possible future work are stated in Section V.

II. Minimum Safety-Factor Dynamics

A magnetic-flux surface is defined by points with the same value of poloidal magnetic flux, Ψ. The poloidal magnetic flux at a point P is defined as $\Psi \triangleq \int_S \vec{B}_\theta \cdot d\vec{S}$, where $\vec{B}_\theta$ is the poloidal magnetic field, and S is the surface normal to the z axis whose boundary is the toroidal ring passing through P, as depicted in Fig. 1. Similarly, the toroidal magnetic flux, Φ, is defined as $\Phi \triangleq \int_{S_\phi} \vec{B}_\phi \cdot d\vec{S}_\phi$, where $\vec{B}_\phi$ is the toroidal magnetic field, and S_ϕ is the surface normal to the ϕ axis whose boundary is the magnetic-flux surface containing P. Under ideal MHD equilibrium conditions [1], the magnetic-flux surfaces are toroidally nested around the magnetic axis (see Fig. 1). The magnetic-flux surfaces can be labeled by a single coordinate within the r-z plane, like Ψ, Φ, or a related variable. This fact and the assumption of toroidal symmetry reduce the 3D problem in space to a 1D problem.

The spatial coordinate employed in this work is the mean effective minor radius, $\rho \triangleq \sqrt{\Phi/(B_{\phi,0}\pi)}$, where $B_{\phi,0}$ is the vacuum toroidal magnetic field at the major radius, R_0. A normalized version of ρ is given by $\hat{\rho} \triangleq \rho/\rho_b$, where ρ_b is the mean effective minor radius of the last-closed magnetic-flux surface. The safety factor, q, is defined as

$$q \triangleq -\frac{d\Phi}{d\Psi} = -\frac{B_{\phi,0}\rho_b^2\hat{\rho}}{\partial\psi/\partial\hat{\rho}}, \tag{1}$$

where $\psi = \Psi/(2\pi)$ is the poloidal stream function. The

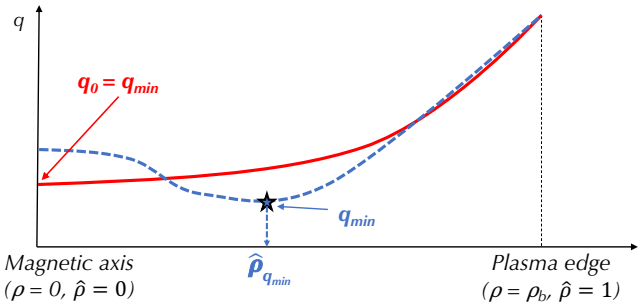

Fig. 2. Examples of typical q-profile shapes in tokamak plasmas. In monotonically increasing q profiles (solid red), q_{min} is found at the magnetic axis, so $\hat{\rho}_{q_{min}} = 0$ and $q_{min} \equiv q_0$. In reverse-shear q profiles (dashed blue), q_{min} is found at an off-axis location, $\hat{\rho}_{q_{min}} \neq 0$.

minimum safety factor, q_{min}, is defined as

$$q_{min} \triangleq q(\hat{\rho}_{q_{min}}), \tag{2}$$

where $\hat{\rho}_{q_{min}}$ is the value of $\hat{\rho}$ where the minimum safety factor is located (see Fig. 2). The dynamics of q_{min} can be characterized through ψ, which is given by the magnetic diffusion equation (MDE) [14],

$$\frac{\partial\psi}{\partial t} = \frac{\eta}{\mu_0\rho_b^2\hat{F}^2}\frac{1}{\hat{\rho}}\frac{\partial}{\partial\hat{\rho}}\left(\hat{\rho}D_\psi\frac{\partial\psi}{\partial\hat{\rho}}\right) + R_0\hat{H}\eta j_{ni}, \tag{3}$$

$$[\partial\psi/\partial\hat{\rho}]_{\hat{\rho}=0} = 0, \quad [\partial\psi/\partial\hat{\rho}]_{\hat{\rho}=1} = -k_{I_p}I_p, \tag{4}$$

where η is the plasma resistivity, j_{ni} is the non-inductive current, $\hat{F}(\hat{\rho})$, $\hat{G}(\hat{\rho})$, $\hat{H}(\hat{\rho})$, $D_\psi \triangleq \hat{F}\hat{G}\hat{H}$, and k_{I_p} are profiles and scalars corresponding to a particular plasma equilibrium, μ_0 is the vacuum permeability, and I_p is the plasma current.

The model described by (1)-(4) is a nonlinear model whose state equation (3) is a partial differential equation with state $\psi(\hat{\rho},t)$ and boundary conditions given by (4), and an output equation defined by (1)-(2). The parameters and profiles $B_{\phi,0}$, ρ_b, R_0, $\hat{F}$, $\hat{G}$, and $\hat{H}$ are assumed to be known exactly, whereas the control-oriented models employed for η and j_{ni} [15] are assumed to contain some level of uncertainty.

The model for η is given by

$$\eta = g_\eta(\hat{\rho})\left(I_p\sqrt{P_{tot}}\bar{n}_e^{-1}\right)^{-3/2} + \delta_\eta, \tag{5}$$

where g_η is a profile characterizing the spatial distribution of the plasma resistivity, P_{tot} is the total injected power, $P_{tot} = \sum_{i=1}^{N_{NB}} P_{NB,i} + P_{EC}$ (where $P_{NB,i}$ denotes the power of the i-th NBI, for $i = 1, ..., N_{NB}$, N_{NB} is the total number of NBI's, and P_{EC} is the EC power), $\bar{n}_e$ is the line-average electron density, and δ_η is an uncertainty. In this work, $P_{NB,i}$ and P_{EC} are considered controllable inputs (I_p and $\bar{n}_e$ are considered non-controllable inputs).

The model for j_{ni} is given by

$$\eta j_{ni} = \sum_{i=1}^{i=N_{NB}} \frac{g_{NB,i}(\hat{\rho})}{I_p\sqrt{P_{tot}}}P_{NB,i} + \frac{g_{EC}(\hat{\rho})}{(I_p\sqrt{P_{tot}}\bar{n}_e)^{1/2}}P_{EC}$$
$$+ (\partial\psi/\partial\hat{\rho})^{-1}g_{BS}(\hat{\rho})(I_p\sqrt{P_{tot}}\bar{n}_e^{-1})^{-1/2}\bar{n}_e + \delta_{j_{ni}}, \tag{6}$$

where $g_{NB,i}$, g_{EC}, and g_{BS} are model profiles related to the NBI, EC, and bootstrap current depositions, respectively, and $\delta_{j_{ni}}$ is an uncertainty.

Using (5) and (6), and taking derivative with respect to $\hat{\rho}$ (see Appendix I for details), (3) can be rewritten as

$$\frac{\partial\theta}{\partial t}=\left(h_{\eta,1}\frac{\partial^2\theta}{\partial\hat{\rho}^2}+h_{\eta,2}\frac{\partial\theta}{\partial\hat{\rho}}+h_{\eta,3}\theta\right)u_\eta+\sum_{i=1}^{N_{NB}}h_{NB,i}u_{NB,i}+h_{EC}u_{EC}+\left(\frac{h_{BS,1}}{\theta}-\frac{h_{BS,2}}{\theta^2}\frac{\partial\theta}{\partial\hat{\rho}}\right)u_{BS}+\delta_\theta, \quad (7)$$

where $\theta(\hat{\rho},t)\triangleq\partial\psi(\hat{\rho},t)/\partial\hat{\rho}$ is the poloidal-flux gradient, $h_{(\cdot)}$ are spatial functions that depend only on $\hat{\rho}$, δ_θ is a term that depends on the uncertainties δ_η and $\delta_{j_{ni}}$, and $u_{(\cdot)}$ are the virtual inputs to the system, i.e., they are functions of the physical inputs, namely, I_p, $P_{NB,i}$ $(i=1,...,N_{NB})$, P_{EC}, and $\bar{n}_e$, as given by

$$u_\eta\triangleq\left(I_p\sqrt{P_{tot}}\bar{n}_e^{-1}\right)^{-\frac{3}{2}},\ u_{NB,i}\triangleq\frac{P_{NB,i}}{I_p\sqrt{P_{tot}}}, \quad (8)$$

$$u_{EC}\triangleq\frac{P_{EC}}{\left(I_p\sqrt{P_{tot}}\bar{n}_e\right)^{\frac{1}{2}}},u_{BS}\triangleq\left(I_p\sqrt{P_{tot}}\bar{n}_e^{-1}\right)^{-\frac{1}{2}}\bar{n}_e. \quad (9)$$

To simplify the notation, the following variables are defined

$$\theta_{q_{min}}\triangleq-\frac{B_{\phi,0}\rho_b^2\hat{\rho}_{q_{min}}}{q_{min}}, \quad (10)$$

$$\theta'_{q_{min}}\triangleq\left[\partial\theta/\partial\hat{\rho}\right]_{\hat{\rho}_{q_{min}}},\ \theta''_{q_{min}}\triangleq\left[\partial^2\theta/\partial\hat{\rho}^2\right]_{\hat{\rho}_{q_{min}}}, \quad (11)$$

Particularizing (7) at $\hat{\rho}_{q_{min}}$ yields

$$\frac{d\theta_{q_{min}}}{dt}=\left[h_{\eta,1}^{min}\theta''_{q_{min}}+h_{\eta,2}^{min}\theta'_{q_{min}}+h_{\eta,3}^{min}\theta_{q_{min}}\right]u_\eta+\sum_{i=1}^{N_{NB}}h_{NB,i}^{min}u_{NB,i}+h_{EC}^{min}u_{EC}+\left(h_{BS,1}^{min}\frac{1}{\theta_{q_{min}}}-h_{BS,2}^{min}\frac{\theta'_{q_{min}}}{\theta_{q_{min}}^2}\right)u_{BS}+\delta_\theta^{q_{min}}, \quad (12)$$

where $h_{\eta,j}^{min}\triangleq h_{\eta,j}(\hat{\rho}_{q_{min}})$ $(j=1,2,3)$, $h_{NB,i}^{min}\triangleq h_{NB,i}(\hat{\rho}_{q_{min}})$ $(i=1,...,N_{NB})$, $h_{EC}^{min}\triangleq h_{EC}(\hat{\rho}_{q_{min}})$, $h_{BS,k}^{min}\triangleq h_{BS,k}(\hat{\rho}_{q_{min}})$ $(k=1,2)$, and $\delta_\theta^{q_{min}}\triangleq\delta_\theta(\hat{\rho}_{q_{min}})$. It must be noted that $\hat{\rho}_{q_{min}}$ is a function of time, so $h_{(\cdot)}^{min}$ also change with time and (12) is a non-autonomous system.

III. Control Synthesis

For control-synthesis purposes, it is considered that real-time estimates or measurements for $\hat{\rho}_{q_{min}}$ and θ are available (e.g., from a real-time equilibrium reconstruction, as is the case in many tokamaks and in DIII-D [16] in particular). This allows for treating $\hat{\rho}_{q_{min}}$ as a known variable (i.e., as a measurable but not directly controllable input), so that (12) can be updated in real time.

Moreover, from (10), it can be noted that regulating q_{min} becomes equivalent to regulating $\theta_{q_{min}}$ as long as $\hat{\rho}_{q_{min}}$ is known. As a result, the control objective can be stated as driving $\theta_{q_{min}}$ towards a real-time-varying target, $\bar{\theta}_{q_{min}}$, so that q_{min} is driven towards a desired target value $\bar{q}_{min}$ that is prescribed off-line. Using the definition (10), the value of $\bar{\theta}_{q_{min}}$ can be calculated in real time as

$$\bar{\theta}_{q_{min}}=-\frac{B_{\phi,0}\rho_b^2\hat{\rho}_{q_{min}}}{\bar{q}_{min}}. \quad (13)$$

It must be noted, from the definition of q_{min} (1)-(2) and the ψ dynamics (3)-(4), that the dynamics of q_{min} and $\hat{\rho}_{q_{min}}$ are not only highly coupled but also dependent on both ψ and q. In the effort of regulating q_{min}, the whole q profile, and $\hat{\rho}_{q_{min}}$, can therefore change in response to the actuation of the controllable inputs. In this work, $\hat{\rho}_{q_{min}}$ is treated as a measurable input rather than modeling its response to the controllable inputs. As a consequence, (12) is updated as $\hat{\rho}_{q_{min}}$ evolves. This approach demands that the update of (13) in real-time implementations be faster than the dynamics of $\hat{\rho}_{q_{min}}$, which guarantees a calculation of $\bar{\theta}_{q_{min}}$ that actually makes q_{min} converge toward $\bar{q}_{min}$.

After these initial considerations, the control-synthesis process for the q_{min} controller has two steps. First, a nominal control law for the nominal system dynamics (i.e., (12) with $\delta_\theta^{q_{min}}=0$) is obtained using Lyapunov theory. Second, a robust control law for the uncertain system dynamics (i.e., (12) with $\delta_\theta^{q_{min}}\neq 0$) is designed based on the nominal control law and Lyapunov redesign techniques. After the q_{min} controller is synthesized, the W controller is briefly introduced, and the overall control scheme for simultaneously regulating q_{min} and W is presented.

A. Nominal Control Law for q_{min}

By setting $d\theta_{q_{min}}/dt$ in (12) with $\delta_\theta^{q_{min}}\equiv 0$ as

$$\frac{d\theta_{q_{min}}}{dt}\triangleq-K_P\tilde{\theta}_{q_{min}}-K_I\int_{t_0}^{t}\tilde{\theta}_{q_{min}}dt+\frac{d\bar{\theta}_{q_{min}}}{dt}, \quad (14)$$

where $K_P>0$, $K_I>0$ are design parameters, and $\tilde{\theta}_{q_{min}}\triangleq\theta_{q_{min}}-\bar{\theta}_{q_{min}}$ is the deviation variable, the nominal system dynamics (i.e., (12) with $\delta_\theta^{q_{min}}\equiv 0$) can be rewritten as

$$\dot{x}_1=-K_Px_1-K_Ix_2,\ \ \dot{x}_2=x_1, \quad (15)$$

where $x=[x_1,x_2]^T\triangleq[\tilde{\theta}_{q_{min}},\int_0^t\tilde{\theta}_{q_{min}}dt]^T$ is the state vector, and $\dot{(\cdot)}\triangleq d(\cdot)/dt$. In order to demonstrate the asymptotical stability of the nominal system dynamics (15), a Lyapunov function [12] given by $V=\frac{1}{2}x_1^2+\frac{1}{2}ax_2^2+bx_1x_2$ is employed, where a and b are constant coefficients that are determined next. First, in order to have $V>0$ for all $x_1\neq 0$, $x_2\neq 0$, the following inequality must be satisfied

$$a-b^2>0. \quad (16)$$

Second, the time derivative of V is given by

$$\dot{V}=-(K_P-b)x_1^2-K_Ibx_2^2-(K_Pb+K_I-a)x_1x_2. \quad (17)$$

In order to make $W\triangleq(K_P-b)x_1^2+K_Ibx_2^2+(K_Pb+K_I-a)x_1x_2>0$ $(\forall x\neq 0)$, the inequalities

$$K_P-b>0,\ \ (K_P-b)K_Ib-\frac{1}{4}(K_Pb+K_I-a)^2>0, \quad (18)$$

must be fulfilled. The constants a and b must be chosen so that (16) and (18) are fulfilled. Taking $a=K_I$, the inequalities in (16) and (18) can be expressed as

$$b<\sqrt{K_I},\ b<K_P,\ b\left(K_PK_I-(K_I+\frac{K_P^2}{4})b\right)>0,$$

where b must fulfill $b > 0$ and $b < K_P K_I/(K_I + \frac{1}{4}K_P^2)$ simultaneously. Therefore, $a = K_I$ and $0 < b < \min\left(\sqrt{K_I}, K_P, K_P K_I/(K_I + \frac{1}{4}K_P^2)\right)$ can be used to prove the asymptotical stability of the nominal system dynamics (15) [12]. Although linear techniques could also have been used, the search of V are motivated by the fact that a nonlinear, robust-control design can be attained using Lyapunov redesign, as shown in Section III-B.

The nominal control law is obtained by equating the right-hand sides of (12) and (14), i.e.,

$$\left[h_{\eta,1}^{min}\theta''_{q_{min}} + h_{\eta,2}^{min}\theta'_{q_{min}} + h_{\eta,3}^{min}\theta_{q_{min}}\right]u_\eta + \sum_{i=1}^{N_{NB}} h_{NB,i}^{min} u_{NB,i} + h_{EC}^{min} u_{EC} + \left(h_{BS,1}^{min}\frac{1}{\theta_{q_{min}}} - h_{BS,2}^{min}\frac{\theta'_{q_{min}}}{\theta_{q_{min}}^2}\right)u_{BS} = = -K_P\tilde{\theta}_{q_{min}} - K_I\int_{t_0}^{t}\tilde{\theta}_{q_{min}}dt + \frac{d\bar{\theta}_{q_{min}}}{dt}. \quad (19)$$

and solving this nonlinear equation (19) for $P_{NB,i}$ ($i = 1, ..., N_{NB}$) and P_{EC}. It can be noted that (19) depends on $P_{NB,i}$ and P_{EC} through u_η, $u_{NB,i}$, u_{EC}, and u_{BS}, as specified by (8)-(9). Because, in general, the number of unknowns, $N_{NB}+1$, is greater than 1, equation (19) by itself does not provide a unique solution for $P_{NB,i}$ and P_{EC}. This issue is addressed in Section III-C.

B. Robust Control Law for q_{min}

In order to robustify the nominal control law by means of Lyapunov redesign techniques [12], a design term v is added to the right-hand side of equation (19),

$$\left[h_{\eta,1}^{min}\theta''_{q_{min}} + h_{\eta,2}^{min}\theta'_{q_{min}} + h_{\eta,3}^{min}\theta_{q_{min}}\right]u_\eta + \sum_{i=1}^{N_{NB}} h_{NB,i}^{min} u_{NB,i} + h_{EC}^{min} u_{EC} + \left(h_{BS,1}^{min}\frac{1}{\theta_{q_{min}}} - h_{BS,2}^{min}\frac{\theta'_{q_{min}}}{\theta_{q_{min}}^2}\right)u_{BS} = = -K_P\tilde{\theta}_{q_{min}} - K_I\int_{t_0}^{t}\tilde{\theta}_{q_{min}}dt + \frac{d\bar{\theta}_{q_{min}}}{dt} + v. \quad (20)$$

where u_η, $u_{NB,i}$, u_{EC}, and u_{BS} are given by (8)-(9). Under the robust control law (20), the uncertain dynamics (i.e., (12) with $\delta_\theta^{q_{min}} \neq 0$) can be rewritten as

$$\dot{x}_1 = -K_P x_1 - K_I x_2 + v + \delta_\theta^{q_{min}}, \quad \dot{x}_2 = x_1. \quad (21)$$

Using the Lyapunov function V from Section III-A with $a = K_I$ and $0 < b < \min\left(\sqrt{K_I}, K_P, K_P K_I/(K_I + \frac{1}{4}K_P^2)\right)$, its time derivative $\dot{V}$ can be bounded as

$$\dot{V} = -W + (x_1 + bx_2)(v + \delta_\theta^{q_{min}}) \leq \leq -W + (x_1 + bx_2)v + |x_1 + bx_2|\delta_\theta^{max}, \quad (22)$$

and if v is chosen as

$$v = -\delta_\theta^{max}\text{sign}(x_1 + bx_2), \quad (23)$$

where δ_θ^{max} is the maximum value attainable for $\delta_\theta^{q_{min}}$, which is assumed to be known, then $\dot{V} \leq -W$. Using the same arguments as in Section III-A, it can be concluded that the uncertain system (21) is asymptotically stable.

The control law (20) with v given by (23) is discontinuous and undefined at $\|x\|_2 \to 0$. Thus, v is modified as follows. First, the region $|x_1 + bx_2| \geq \epsilon/\delta_\theta^{max}$ is considered, where $\epsilon > 0$ is a design parameter. In such region, $v = \text{sign}(x_1 + bx_2)$ is always defined, and $\dot{V} \leq -W$. When $|x_1 + bx_2| < \epsilon/\delta_\theta^{max}$, taking $v = -(x_1 + bx_2)(\delta_\theta^{max})^2/\epsilon$ yields

$$\dot{V} \leq -W - (x_1 + bx_2)^2(\delta_\theta^{max})^2/\epsilon + |x_1 + bx_2|\delta_\theta^{max}. \quad (24)$$

It can be noted that the two last terms on the right-hand side of (24) can be written as $f(w) = -\frac{w^2}{\epsilon} + w$, with $w = \delta_\theta^{max}|x_1 + bx_2|$. A maximum at $w_{max} = \epsilon/2$ if found for $f(w)$, at which $f(w_{max}) = \epsilon/4$. Therefore, (24) can be rewritten as $\dot{V} \leq -W + \epsilon/4$, which, because $\epsilon > 0$, is fulfilled not only when $|x_1 + bx_2| < \epsilon/\delta_\theta^{max}$, but also when $|x_1 + bx_2| \geq \epsilon/\delta_\theta^{max}$. This allows for concluding that x is ultimately bounded as $\|x\|_2 \leq g_B(\epsilon)$ [12], where g_B is a class $\mathcal{K}$ function[1]. To have a bound that is as tight as possible, it is necessary to set ϵ small ($\epsilon \to 0$).

The robust control law is obtained from by solving (20) for $P_{NB,i}$ ($i = 1, ..., N_{NB}$) and P_{EC}, with v given by

$$v = -\delta_\theta^{max}\text{sign}(x_1 + bx_2), \quad \text{if } |x_1 + bx_2| \geq \epsilon/\delta_\theta^{max}, \quad (25)$$

$$v = -(\delta_\theta^{max})^2(x_1 + bx_2)/\epsilon, \quad \text{if } |x_1 + bx_2| < \epsilon/\delta_\theta^{max}. \quad (26)$$

As in the nominal case, the number of unknowns, $N_{NB}+1$, is in general greater than 1, so equation (20) by itself does not provide a unique solution for $P_{NB,i}$ and P_{EC}. This issue is addressed in Section III-C.

C. Integration of the q_{min} and W Control Laws

As introduced at the end of Sections III-A and III-B, the q_{min} control law does not univocally determine the vector of controllable inputs $P = [P_{NB,1}, ..., P_{NB,N_{NB}}, P_{EC}]^T$. This makes the q_{min} controller suitable for integration with other controllers. In particular, it is often desired to regulate the plasma thermal energy, W, which is proportional to the plasma pressure. Although the details are not shown in this work, a nonlinear robust control law for W that follows the derivation in [13] is employed. This controller determines the total injected power, P_{tot}^{req}, required for W regulation. P_{tot}^{req}, which is calculated at each time step from W and its target $\bar{W}$, must at all time satisfy

$$\sum_i P_{NB,i} + P_{EC} = P_{tot}^{req}. \quad (27)$$

It is, therefore, considered in this work that P_{tot}^{req} is a known variable that is computed in real time by the W controller.

The components of $P = [P_{NB,1}, ..., P_{NB,N_{NB}}, P_{EC}]^T \in \mathbb{R}^{N_{NB}+1}$ are determined by solving a real-time optimization problem,

$$\min_P P^T Q P \quad (28)$$

$$\text{subject to (20), (27), and saturation limits on } P, \quad (29)$$

where $Q > 0$ is a diagonal matrix whose terms are chosen by design, so the control effort $P^T Q P$ is minimized. The problem (28)-(29) is solved using a sequential quadratic-programming algorithm [17].

[1] $f(x)$ is class $\mathcal{K}$ iff: (1) $f(0) = 0$, (2) it is strictly increasing with x.

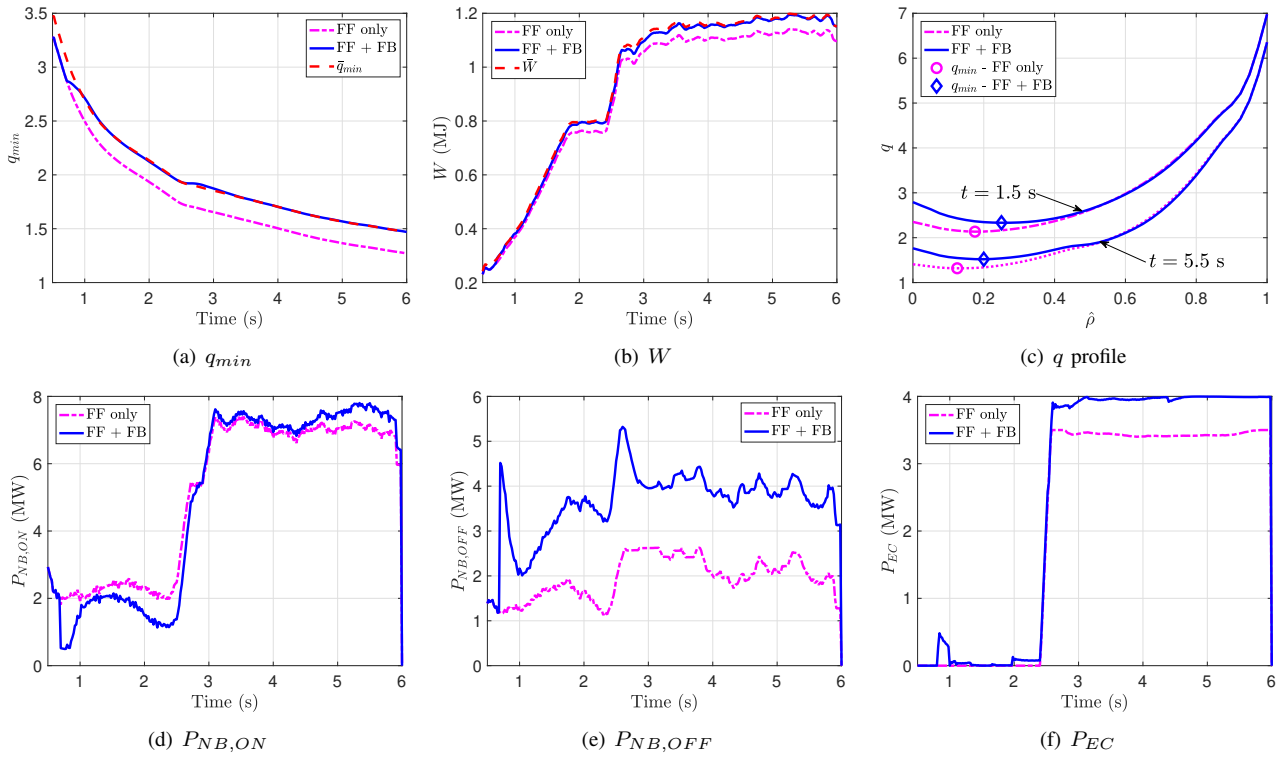

(a) q_{min} (b) W (c) q profile

(d) $P_{NB,ON}$ (e) $P_{NB,OFF}$ (f) P_{EC}

Fig. 3. Simulation results using COTSIM in FF-only (magenta dashed-dotted) and FF + FB (blue solid) simulations, together with the targets (red dashed). The system outputs (q_0, W) and controllable inputs ($P_{NB,ON}$, $P_{NB,OFF}$, and P_{EC}) are plotted together with the q profile at $t = 1.5$ s and $t = 5.5$ s.

IV. Simulation Study

In this section, the control algorithm previously introduced is tested in 1D simulations for the DIII-D tokamak. Two types of NBIs are used (i.e., $N_{NB} = 2$): on-axis NBIs and off-axis NBIs, whose powers are denoted by $P_{NB,ON}$ and $P_{NB,OFF}$, respectively. The saturation limits are $P_{NB,(\cdot)} \in [0, 3]$ MW and $P_{EC} \in [0, 4]$ MW. The simulation study is carried out by means of COTSIM, which is a 1D code for control testing and simulation that evolves ψ using the MDE (3) together with the electron heat-transport equation for the electron temperature, T_e, as given by

$$\frac{\partial(\frac{3}{2}n_e T_e)}{\partial t} = \frac{1}{\rho_b^2 \hat{\rho} \hat{H}} \frac{\partial}{\partial \hat{\rho}} \left(\hat{\rho} \frac{\hat{G}\hat{H}^2}{\hat{F}} \chi_e n_e \frac{\partial T_e}{\partial \hat{\rho}} \right) + Q_e, \quad (30)$$

where χ_e is the electron heat diffusivity and Q_e is the electron-heat deposition. Control-oriented models are used for n_e, j_{ni}, and Q_e, and a Spitzer-like model is used for η, i.e., $\eta \propto T_e^{-3/2}$. A Bohm/Gyro-Bohm model [18] is used for χ_e. Then, the MDE and electron heat-transport are coupled by means of the diffusive terms (η and χ_e) and source terms (j_{ni} and Q_e). Analytical models are used to estimate the pedestal evolution [19], so the core and pedestal transport are coupled. The use in simulations of (30) with a Bohm/Gyro-Bohm model in combination with an analytical pedestal model represents a significant increase in model complexity when compared with those models used for control synthesis in Section II, where the dynamics of T_e is neglected.

The objective of this section is to assess the performance of the q_{min} + W control scheme in the presence of unknown plasma dynamics while simultaneously driving both W and q_{min} toward their respective targets, $\bar{W}$ and $\bar{q}_{min}$. First, a feedforward-only simulation is run with the experimental inputs from shot 172538. The evolutions of q_{min} and W in such simulation are denoted by q_{min}^{exp} and W^{exp}, respectively. These are employed to generate the targets for a FF + FB simulation. The targets are set as $\bar{q}_{min} = q_{min}^{exp} + 0.2$ and $\bar{W} = 1.05W^{exp}$. Then, a FF + FB simulation is executed, and the FB controller is activated at $t = 0.7$ s.

Fig. 3 shows the time evolutions of q_{min}, W, $\bar{q}_{min}$ and $\bar{W}$, together with the q profile at $t = 1.5$ s and $t = 5.5$ s, as well as the controllable inputs, $P_{NB,ON}$, $P_{NB,OFF}$, and P_{EC}, during the FF and FF + FB simulations. It can be seen that good performance is achieved when regulating q_{min} and W, which converge toward $\bar{q}_{min}$ and $\bar{W}$ ((see Fig. 3(a)) and Fig. 3(b), respectively). To achieve so, the W controller increases $P_{tot}^{req} = P_{NB,ON} + P_{NB,OFF} + P_{EC}$, and the q_{min} controller initially increases $P_{NB,OFF}$ (see Fig. 3(e)), moderately increases P_{EC} (see Fig. 3(f)), and decreases $P_{NB,ON}$ (see Fig. 3(d)), so that q_{min} is increased. Later during the simulation, at $t \approx 3$ s, $P_{NB,ON}$ is also increased to drive W toward $\bar{W}$. It can be observed that the overall q-profile shape and $\hat{\rho}_{q_{min}}$ change (see Fig. 3(c)) by regulating q_{min} and W. There is an increase in the q profile in the central plasma region. Also, a more negative magnetic shear is attained in the FF + FB simulation than in the FF simulation, as a result of achieving a higher $\hat{\rho}_{q_{min}}$. The negative magnetic shear may improve the plasma confinement [1], facilitating the regulation of W around $\bar{W}$.

V. Conclusion and Possible Future Work

A nonlinear-robust controller for q_{min} in tokamaks has been presented. Its synthesis process is based on the use of Lyapunov theory and redesign techniques. It also assumes that an estimate for the location of q_{min} is available, which is a standard capability in present tokamaks. Moreover, as the q_{min} controller works by specifying a constraint for the controllable inputs, rather than computing the inputs directly, it can be easily integrated with other controllers. In conjunction with a W controller, the q_{min} controller shows good performance and robustness in the presence of unknown dynamics in simulations using COTSIM. Future work may include experimental testing of the controller in DIII-D.

Appendix I

Using the definition of the poloidal-flux gradient, $\theta \triangleq \partial\psi/\partial\hat{\rho}$, and applying the chain rule, (7) is rewritten as

$$\frac{\partial\psi}{\partial t} = \frac{\eta}{\mu_0\rho_b^2\hat{F}^2}\left[D_\psi\theta' + \left(\frac{D_\psi}{\hat{\rho}} + D'_\psi\right)\theta\right] + R_0\hat{H}\eta j_{ni},$$

where $(\cdot)' \triangleq \partial(\cdot)/\partial\hat{\rho}$, and taking time derivative yields

$$\begin{aligned}\frac{\partial\theta}{\partial t} &= \left(\frac{\eta}{\mu_0\rho_b^2\hat{F}^2}\right)'\left[D_\psi\theta' + \left(\frac{D_\psi}{\hat{\rho}} + D'_\psi\right)\theta\right] \\ &+ \frac{\eta}{\mu_0\rho_b^2\hat{F}^2}\left[D_\psi\theta'' + \left(\frac{D_\psi}{\hat{\rho}} + 2D'_\psi\right)\theta' + \left(\frac{D'_\psi\hat{\rho} - D_\psi}{\hat{\rho}^2}\right)\theta\right] \\ &+ \left(R_0\hat{H}\eta j_{ni}\right)'. \end{aligned} \quad (31)$$

Using (5), reorganizing the terms in (31) yields

$$\begin{aligned}\frac{\partial\theta}{\partial t} &= \frac{1}{\mu_0\rho_b^2}\left\{\left[\left(\frac{g_\eta}{\hat{F}^2}\right)'\left(\frac{D_\psi}{\hat{\rho}} + D'_\psi\right) + \frac{g_\eta}{\hat{F}^2}\left(\frac{D'_\psi\hat{\rho} - D_\psi}{\hat{\rho}^2}\right)\right]\theta\right. \\ &+ \left[\left(\frac{g_\eta}{\hat{F}^2}\right)'D_\psi + \frac{g_\eta}{\hat{F}^2}\left(\frac{D_\psi}{\hat{\rho}} + 2D'_\psi\right)\right]\theta' \\ &\left.+ \frac{g_\eta}{\hat{F}^2}D_\psi\theta''\right\}(I_p\sqrt{P_{tot}}\bar{n}_e^{-1})^{-\frac{3}{2}} + \left(R_0\hat{H}\eta j_{ni}\right)' \\ &+ \left(\frac{\delta_\eta}{\mu_0\rho_b^2\hat{F}^2}\left[D_\psi\theta' + \left(\frac{D_\psi}{\hat{\rho}} + D'_\psi\right)\theta\right]\right)' u_\eta. \end{aligned} \quad (32)$$

The term $\left(R_0\hat{H}\eta j_{ni}\right)'$ in equation (32) can be rewritten, using (6) and applying the chain rule, as

$$\begin{aligned}\left(R_0\hat{H}\eta j_{ni}\right)' &= R_0\sum_i(\hat{H}g_{NB,i})'(I_p\sqrt{P_{tot}})^{-1}P_{NB,i} \\ &+ R_0(\hat{H}g_{EC})'(I_p\sqrt{P_{tot}}\bar{n}_e^{-1})^{(-1/2)}\bar{n}_e^{-1}P_{EC} \\ &+ R_0(\hat{H}g_{BS})'(I_p\sqrt{P_{tot}}\bar{n}_e^{-1})^{-1/2}\bar{n}_e + R_0(\hat{H}\delta_{j_{ni}})'. \end{aligned}$$

By defining the following model profiles,

$$h_{\eta,1} \triangleq \frac{1}{\mu_0\rho_b^2}\frac{g_\eta}{\hat{F}^2}D_\psi, \quad (33)$$

$$h_{\eta,2} \triangleq \frac{1}{\mu_0\rho_b^2}\left[\left(\frac{g_\eta}{\hat{F}^2}\right)'D_\psi + \frac{g_\eta}{\hat{F}^2}\left(\frac{D_\psi}{\hat{\rho}} + 2D'_\psi\right)\right], \quad (34)$$

$$h_{\eta,3} \triangleq \frac{1}{\mu_0\rho_b^2}\left[\left(\frac{g_\eta}{\hat{F}^2}\right)'\left(\frac{D_\psi}{\hat{\rho}} + D'_\psi\right) + \frac{g_\eta}{\hat{F}^2}\left(\frac{D'_\psi\hat{\rho} - D_\psi}{\hat{\rho}^2}\right)\right],$$

$$h_{NB,i} \triangleq R_0(\hat{H}g_{NB,i})',\ h_{EC} \triangleq R_0(\hat{H}g_{EC})',$$

$$h_{BS,1} \triangleq R_0(\hat{H}g_{BS})',\ h_{BS,2} \triangleq R_0\hat{H}g_{BS},$$

the virtual inputs in (8)-(9), and the uncertainty

$$\delta_\theta \triangleq \left(\frac{\delta_\eta}{\mu_0\rho_b^2\hat{F}^2}\left[D_\psi\theta' + \left(\frac{D_\psi}{\hat{\rho}} + D'_\psi\right)\theta\right]\right)' u_\eta + R_0(\hat{H}\delta_{j_{ni}})',$$

equation (32) becomes

$$\begin{aligned}\frac{\partial\theta}{\partial t} &= \left(h_{\eta,1}\frac{\partial^2\theta}{\partial\hat{\rho}^2} + h_{\eta,2}\frac{\partial\theta}{\partial\hat{\rho}} + h_{\eta,3}\theta\right)u_\eta + \sum_{i=1}^{N_{NB}} h_{NB,i}u_{NB,i} \\ &+ h_{EC}u_{EC} + \left(h_{BS,1}\frac{1}{\theta} - h_{BS,2}\frac{\partial\theta/\partial\hat{\rho}}{\theta^2}\right)u_{BS} + \delta_\theta. \end{aligned}$$

References

[1] J. Wesson, *Tokamaks*. Oxford, UK: Clarendon Press, 1984.

[2] T. Suzuki *et al.*, "Off-axis current drive and real-time control of current profile in JT-60U," *Nuclear Fusion*, vol. 48, no. 4, p. 045002, 2008.

[3] B. Argomedo *et al.*, "Model-based control of the magnetic flux profile in a tokamak plasma," in *Decision and Control (CDC), 2010 49th IEEE Conference on*, 2010, pp. 6926–6931.

[4] J. Barton *et al.*, "Physics-model-based nonlinear actuator trajectory optimization and q-profile feedback control for advanced scenario development in DIII-D," *Nucl. Fusion*, vol. 55, no. 093005, 2015.

[5] F. Felici *et al.*, "Enhancing current density profile control in tokamak experiments using iterative learning control," in *2015 54th IEEE Conference on Decision and Control (CDC)*, 2015, pp. 5370–5377.

[6] D. Moreau *et al.*, "A two time scale dynamic model approach for magnetic and kinetic profile control in advanced tokamak scenarios on JET," *Nucl. Fusion*, vol. 48, no. 106001, 2008.

[7] E. Maljaars *et al.*, "Control of the tokamak q profile with time-varying constraints using MPC," *Nucl. Fusion*, vol. 55, no. 2, 2015.

[8] W. P. Wehner *et al.*, "Optimal current profile control for enhanced repeatability of L-mode and H-mode discharges in DIII-D," *Fusion Engineering and Design*, vol. 123, pp. 513–517, 2017.

[9] J. Ferron *et al.*, "Feedback Control of the Safety Factor Profile Evolution during Formation of an Advanced Tokamak Discharge," *Nucl. Fusion*, vol. 46, no. 10, p. L13, 2006.

[10] M. Boyer *et al.*, "Central safety factor and β_N control on NSTX-U via beam power and plasma boundary shape modification," *Nucl. Fusion*, vol. 55, 2015.

[11] A. Pajares and E. Schuster, "Central safety factor control in DIII-D using neutral beam injection and electron cyclotron launchers in zero input-torque scenarios," in *IEEE Conference on Control Technology and Applications (CCTA)*, 2017, pp. 1460–1465.

[12] H. Khalil, *Nonlinear Systems*, 3rd ed. NJ: Prentice Hall, 2001.

[13] A. Pajares and E. Schuster, "Integrated robust control of individual scalar variables in tokamaks," in *IEEE Conference on Decision and Control (CDC)*, 2019, pp. 3233–3238.

[14] F. Hinton and R. Hazeltine, "Theory of plasma transport in toroidal confinement systems," *Rev. Mod. Phys.*, vol. 48, pp. 239–308, 1976.

[15] J. Barton *et al.*, "Physics-based control-oriented modeling of the safety factor profile dynamics in high performance tokamak plasmas," *52nd IEEE Conference on Decision and Control*, 2013.

[16] J. Ferron *et al.*, "Real time equilibrium reconstruction for tokamak discharge control," *Nuclear Fusion*, vol. 38, pp. 1055–1066, 1998.

[17] J. Nocedal and S. J. Wright, *Numerical Optimization*, 2nd ed. Springer, 2006.

[18] M. Erba *et al.*, "Validation of a new mixed Bohm/gyro-Bohm model for electron and ion heat transport against the ITER, Tore Supra and START database discharges," *Nucl. Fusion*, vol. 38, 1998.

[19] T. Onjun, G. Bateman, A. H. Kritz, and G. Hammett, "Models for the pedestal temperature at the edge of H-mode tokamak plasmas," *Physics of Plasmas*, vol. 9, no. 5018, 2002.